A tale of two catchments: Causality analysis and isotope systematics reveal mountainous watershed traits that regulate the retention and release of nitrogen

Nick Bouskill[1], Michelle E. Newcomer[2], Rosemary W.H. Carroll[3], Curtis A Beutler[4], Markus Bill[1], Wendy S Brown[4], Mark E Conrad[5], Wenming Dong[6], Nicola Falco[2], Taylor Maavara[7], Alexander Newman[4], Patrick O Sorensen[1], Tetsu K Tokunaga[1], Jiamin Wan[8], Haruko Murakami Wainwright[2], Qing Zhu[2], Eoin Brodie[2], and Kenneth Hurst Williams[2]

[1]Lawrence Berkeley National Laboratory
[2]Lawrence Berkeley National Laboratory (DOE)
[3]Desert Research Institute
[4]Rocky Mountain Biological Laboratory
[5]Lawrence Berkeley Laboratory
[6]Lawrence Berkeley Natiional Laboratory
[7]University of Leeds
[8]Lawrence Berkeley National Lab

May 2, 2023

Abstract

Mountainous watersheds are characterized by variability in functional traits, including vegetation, topography, geology, and geomorphology, which together determine nitrogen (N) retention, and release. Coal Creek and East River are two contrasting catchments within the Upper Colorado River Basin that differ markedly in total nitrate (NO3-) export. The East River has a diverse vegetation cover, sinuous floodplains, and is underlain by N-rich marine shale, resulting in a three to twelve times greater total NO3- export relative to the conifer-dominated Coal Creek. While this can partly be explained by the larger size of the East River, the distinct watershed traits of these two catchments imply different mechanisms controlling the aggregate N-export signal. A causality analysis shows biogenic and geogenic processes were critical in determining NO3- export from the East River catchment. Stable isotope ratios of NO3- (δ15NNO3 and δ18ONO3) show the East River catchment is a strong hotspot for biogeochemical processing of NO3- at the soil-saprolite interface and within the floodplain prior to export. By contrast, the conifer-dominated Coal Creek retained nearly all (˜97 %) atmospherically-deposited NO3-, and its export was controlled by catchment hydrological traits (i.e., snowmelt periods and water table depth). The conservative N-cycle within Coal Creek is likely due to the abundance of conifer trees, and a smaller riparian region, retaining more NO3- overall and reduced processing prior to export. This study highlights the value of integrating isotope systematics to link watershed functional traits to mechanisms of watershed element retention and release.

Hosted file

961356_0_art_file_10936573_rtrwbr.docx available at https://authorea.com/users/530146/articles/640473-a-tale-of-two-catchments-causality-analysis-and-isotope-systematics-reveal-mountainous-watershed-traits-that-regulate-the-retention-and-release-of-nitrogen

Hosted file

961356_0_supp_10904558_rt76hg.docx available at https://authorea.com/users/530146/articles/640473-a-tale-of-two-catchments-causality-analysis-and-isotope-systematics-reveal-mountainous-watershed-traits-that-regulate-the-retention-and-release-of-nitrogen

A tale of two catchments: Causality analysis and isotope systematics reveal mountainous watershed traits that regulate the retention and release of nitrogen

Bouskill NJ[1*], Newcomer M[1], Carroll RWH[2,3], Beutler C[3], Bill M[1], Brown WS[3], Conrad M[1], Dong WS[1], Falco N[1], Maavara T[4], Newman A[3], Sorensen PO[1], Tokunaga TK[1], Wan J[1], Wainwright H[1], Zhu Q[1], Brodie EL[1], Williams KH[1,3]

[1]Earth and Environmental Sciences Area, Lawrence Berkeley National Laboratory, Berkeley, CA, USA.
[2]Desert Research Institute, Reno, NV, USA.
[3]Rocky Mountain Biological Laboratory, Gothic, CO, USA.
[4]School of Geography, University of Leeds, UK.

*Corresponding author: njbouskill@lbl.gov

Abstract

Mountainous watersheds are characterized by variability in functional traits, including vegetation, topography, geology, and geomorphology, which together determine nitrogen (N) retention, and release. Coal Creek and East River are two contrasting catchments within the Upper Colorado River Basin that differ markedly in total nitrate (NO_3^-) export. The East River has a diverse vegetation cover, sinuous floodplains, and is underlain by N-rich marine shale, resulting in a three to twelve times greater total NO_3^- export relative to the conifer-dominated Coal Creek. While this can partly be explained by the larger size of the East River, the distinct watershed traits of these two catchments imply different mechanisms controlling the aggregate N-export signal. A causality analysis shows biogenic and geogenic processes were critical in determining NO_3^- export from the East River catchment. Stable isotope ratios of NO_3^- ($\delta^{15}N_{NO3}$ and $\delta^{18}O_{NO3}$) show the East River catchment is a strong hotspot for biogeochemical processing of NO_3^- at the soil-saprolite interface and within the floodplain prior to export. By contrast, the conifer-dominated Coal Creek retained nearly all (~97 %) atmospherically-deposited NO_3^-, and its export was controlled by catchment hydrological traits (i.e., snowmelt periods and water table depth). The conservative N-cycle within Coal Creek is likely due to the abundance of conifer trees, and a smaller riparian region, retaining more NO_3^- overall and reduced processing prior to export. This study highlights the value of integrating isotope systematics to link watershed functional traits to mechanisms of watershed element retention and release.

Plain Language Summary

The role different functional traits play in the retention and release of nitrogen remains uncertain. Here we describe how two neighboring catchments in the Upper Colorado River Basin, characterized by contrasting vegetation, geology, and geomorphology, cycle and export nitrogen. The East River catchment, which is underlain by nitrogen-rich shale, and has a diverse vegetation cover, releases three to twelve-times as much nitrate (NO_3^-) than the conifer-dominated Coal Creek, which is underlain by granitic rock. However, a suite of analyzes show that the distinct watershed traits of these two-catchments lead to diverse emergent pathways of nitrogen cycling. Biogenic and geogenic processes, critical to determining NO_3^- export in East River, impart strong biogeochemical processing prior to export. By contrast, Coal Creek retains almost all of the atmospherically-deposited NO_3^-, likely due to uptake by conifers, and a small riparian region. This study highlights the use of nitrate isotope systematics to parse different mechanisms leading to NO_3^- export.

Key points

- Comparing and contrasting neighboring catchments permits the identification of watershed traits regulating the cycling, retention and release of nitrogen (N).
- Conifer forest-dominated catchments show a conservative nitrogen cycling, retaining ~97 % of atmospherically dominated nitrate.
- By contrast, meadow-dominated catchments underlain Mancos shale are biogeochemical hotspots for N-cycling, and export higher nitrate loads.

1. Introduction

Strong variability in stream water chemistry between neighboring headwater catchments can provide insight into how watershed traits (e.g., gradients in bedrock, topography, aspect, and land cover) interact to modulate retention and release of critical elements and thus influence downstream water quality (Alexander et al., 2007; McDonnell et al., 2007). Nitrogen, which often limits ecosystem processes within mountainous watersheds (Campbell et al., 2002; Kou et al., 2020; Thébault et al., 2014), enters through several pathways, including by atmospheric deposition of inorganic and organic nitrogen (Clark et al., 2021), bedrock weathering (Holloway et al., 1998; Houlton et al., 2018; Wan et al., 2021), and nitrogen fixation (Moyes et al., 2016). Retention within the ecosystem occurs primarily through plant acquisition, microbial immobilization (Goodale, 2017; Zogg et al., 2000), and groundwater storage (Ascott et al., 2017). Loss of nitrogen occurs through denitrification within variably saturated regions of the watershed (e.g., within floodplains, Bouskill et al., 2019; Gomez-Velez et al., 2015), the erosional deposition of particulate nitrogen (Berhe & Torn, 2017), or lateral flow of dissolved species to streams and rivers (Peterson, 2001; Rose et al., 2015).

The balance between the retention and release of nitrogen in headwater catchments is strongly coupled to the hydrological cycle (Maavara et al., 2021; Wan et al., 2021; Schimel et al., 1997; Zhu et al., 2018). The transit times of different solutes through the terrestrial biosphere are dictated by the contact time between water and reactive surfaces including microorganisms (Lansdown et al., 2015; Li et al., 2021; Pinay et al., 2015). The resultant stream water chemistry is derived from distinct water sources that reflect this transit time, and the magnitude of biogeochemical cycling of nitrogen along the various flow paths to the river. Depending on the time of year within snowmelt-dominated systems, the chemical signatures might reflect nitrogen derived from flow paths across distinct hillslope depths (Zhi et al., 2019; Zhi et al., 2020), whereby shallow soils dominate solute flux to the river as the water table rises towards the surface during snowmelt (Zhi et al., 2019). By contrast, stream water chemistry likely reflects the deeper groundwater-dominated sources under baseflow conditions.

The movement of water and nitrogen through the subsurface of mountainous catchments is also further modified through interactions with vegetation. Plant-nitrogen assimilation predominantly takes place from shallow soil layers, aided by the turnover of microbial biomass built-up under snowpack (Sorensen et al., 2020). Mycorrhizal-symbionts further regulate nutrient transfer from soils to plants (Hobbie & Högberg, 2012), and the relationship between plants and different mycorrhizal fungi shapes the nitrogen sources that can be accessed (Phillips et al., 2013; Ward et al., 2022). Moreover, the flux of nitrogen entering catchments is also dependent on litter decomposition is a function of litter quality (e.g., carbon: nitrogen ratios), which is a function of species demographics and a critical pathway of the nitrogen cycle in high-altitude soils (Maavara et al., 2021). Catchment heterogeneity results in the emergence of different plant communities, which, subsequently plays an important role in determining aggregate nitrogen retention and release (Newcomer et al., 2021).

This study details how nitrogen is cycled and exported as a function of headwater catchment traits. We compare and contrast the nitrogen cycles of two catchments, Coal Creek and the main stem East River, within the wider East River watershed in the Upper Colorado River Basin, United States. Although separated by less than 7 kilometers, these snowmelt-dominated catchments differ in their underlying traits, notably geology, dominant vegetation, geomorphology, and aspect (Hubbard et al., 2018). In contrast, rates of atmospheric nitrogen deposition to the two catchments are similar and extremely low (~2-3 kg ha^{-1} yr^{-1}), meaning that underlying catchment traits dominate the differences in nitrogen retention and release. Herein we examine whether the contrasting biotic and abiotic traits that distinguish Coal Creek and the East River are apparent through contrasting signals in nitrogen export.

To test this supposition, we analyze concentration-discharge (cQ) relationships of biogenic and geogenically derived solutes across a five-year data time series from both Coal Creek and East River catchments. cQ relationships have been widely used to determine how different catchments store and release water and solutes (Knapp et al., 2020), and to partition between geogenic and biogenic sources as a function of the hydrograph (Zhi et al., 2019). The cQ relationship is often described by a power law between the logarithms of both variables ($c=aQ^b$), where a represents the intercept and the exponent, b, represents the slope of the cQ relationship

(Musolff et al., 2015). The exponent provides information determining how the relationship between solute export changes with the hydrograph (Thompson et al., 2011). For example, $b = 0$ indicates a chemostatic relationship between discharge and solute concentration, a relationship characteristic of headwater catchments (Godsey et al., 2009). By contrast, positive or negative deviations from this relationship can represent solute mobilization (e.g., from shallow soil reservoirs), or dilution (common for geogenically derived solutes), respectively (Knapp et al., 2020; Musolff et al., 2015; Zhi et al., 2020). However, the power law characterization of the cQ is insensitive to high variability in data, which can be the case for nutrients such as NO_3^- and attributable to heterogeneity in landscape properties and hydrologic connectivity that influence groundwater table fluctuations, redox conditions, and elemental mobility (Thompson et al., 2011). We therefore combine the power law analysis with an analysis of the ratio between the coefficient of variation (CV) of concentration (CV_c) and discharge (CV_c/CV_q), which can further contextualize whether the underlying relationship in solute export is driven by variability in discharge, improving understanding of solute mobilization (Knapp et al., 2022). For example, a CV_c/CV_q ratio ≤ 0.5 indicates that the variability in discharge (CV_q) is greater than the variability in solute concentrations (CV_c), and is therefore, chemostatic. By contrast, a high solute concentration variability, relative to discharge ($CV_c/CV_q \geq 0.5$), the relationship might be considered chemodynamic.

Neither metric described above attributes solute export to an underlying mechanism, therefore this analysis is combined with measurements of the stable isotopes of nitrate ($\delta^{15}N_{NO3}$ and $\delta^{18}O_{NO3}$) from both soil porewater, as well as Coal Creek and East River. The isotopic signature of nitrate represents the aggregated contribution of different sources and reflects both the strength of retention and the magnitude of biogeochemical cycling along different flow paths towards the river (Granger & Wankel, 2016). $\delta^{15}N_{NO3}$ and $\delta^{18}O_{NO3}$ can identify periods of high nitrate reduction through the monotonic enrichment in isotopic fractionation (Wexler et al., 2014), indicating prolonged transit times through the ecosystem. Moreover, the direct contribution of atmospheric nitrate to riverine export can be identified through high $\delta^{18}O_{NO3}$ (~60 - 80 ‰) imparted during the atmospheric formation of nitrate (Michalski et al., 2012), and this isotopic signal can be used to quantify retention of atmospheric nitrate by vegetation and microbes.

We use these complementary data sets to address two main objectives: Our first objective seeks to compare and contrast nitrate export within two neighboring catchments differing in functional trait distribution while sharing the same climate and nitrogen deposition patterns. A second objective focuses on the East River catchment and leverages existing borehole infrastructure, not currently available in Coal Creek, to relate riverine nitrate export to nitrogen cycling across a hillslope-toeslope-floodplain continuum adjoining the river.

2. Materials and Methods

2.1. Study Site: The East River watershed (38° 57.5' N, 106° 59.3' W) is a representative headwater system in the West Elk Mountains near the towns of Crested Butte and Gothic, Colorado (USA) within the Upper Colorado Basin (Hubbard et al., 2018). The East River is a major tributary to the Gunnison River, which accounts for almost half of the Colorado River's discharge at the border with Utah. The East River watershed is approximately 300 km^2 (Fig. 1), and encompasses the main stem East River (including the current study site East River at Pumphouse), Slate River, Washington Gulch, and Coal Creek (Fig. 1a). The East River watershed is a large watershed of the hydrologic unit code 10 (USGS: HUC10 East River Watershed: #1402000102)), characterized by the intersection of two HUC12 catchments. The East River at Pumphouse is made up of the smaller HUC12 catchments (#140200010201 Upper East River) which drains to the HUC12 #140200010202 Brush Creek catchment where the Pumphouse is located. For clarity, the catchment, East River at Pumphouse, is hereafter referred to as ERP, to avoid confusion with the larger East River watershed. Coal Creek is a defined HUC12 catchment (#140200010204 Coal Creek) of the HUC10 East River Watershed (#1402000102).

The East River watershed has an average elevation of 3266 m, and ranges from 2750 to 4000 m (Fig. 1b). The area has a continental, subarctic climate, with a mean annual temperature of 0°C, and average minimum and maximum temperatures of -9.2 and 9.8°C, respectively. Mean annual precipitation is ~1200 mm yr^{-1}, with the majority (> 80 %) falling as snow, and much of the rest falling during the monsoonal period in late summer and fall (Carroll et al., 2020). Snowfall and melt dominate the hydrological cycle, as is typical for mountainous systems in the Western United States (Li et al., 2017), and losses are partitioned between evapotranspiration and streamflow, which differ in their contributions based on several characteristics, including a higher ET flux with higher proportional tree cover (Sprenger et al., 2022). Runoff characteristics for both catchments are similar in terms of the timing of peak discharge in early June and the transition to baseflow in late September-early October, where groundwater represents a significant fraction of streamflow (Hubbard et al., 2018).

Atmospheric deposition of wet and dry forms of reactive nitrogen (nitrate and ammonium) for the East River watershed was extracted from the EPA CASTNET continuous monitoring system located at Gothic (https://www3.epa.gov/castnet/site_pages/GTH161.html), and from the broader national atmospheric deposition program (https://nadp.slh.wisc.edu/committees/tdep/). Annual nitrogen deposition averaged 2 - 3 kg-N ha^{-1} over a 17-year period (2000-2017), split equally between reduced and oxidized inorganic nitrogen (Fig. S1).Over that period the magnitude of total nitrogen deposited into the watershed remained relatively constant, but the contribution from ammonia roughly doubled, while that from nitrate fell, consistent with other regions of the Rocky Mountains (Clark et al., 2021), and likely attributable to a lack of regulation on NH_4^+ emissions (Li et al., 2016).

Figure 1: The East River watershed depicting (a) land cover and (b) elevation. On each panel the different catchments are demarcated by a black outline. With the Coal Creek catchment the river sampling point is denoted by the orange diamond, while the orange circle in the East Tiver catchment indicates the river sampling point, and the adjacent borehole transect for terrestrial porewater collection.

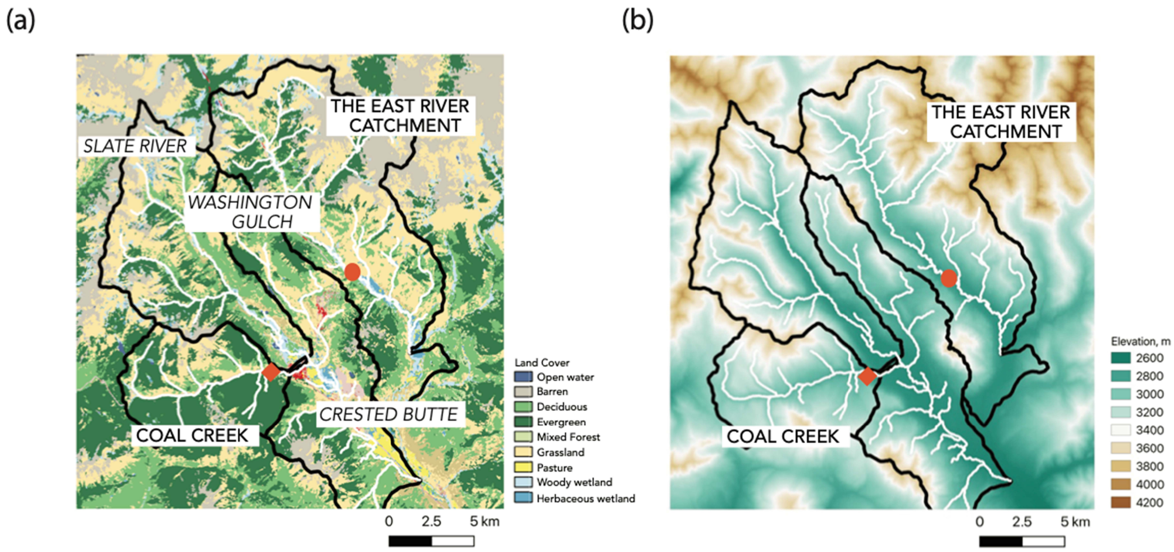

A recent analysis for the wider East River watershed separates these two catchments based on their comparative disparity in traits including catchment size, aspect, average slope, vegetation (including normal difference vegetation index), and geology (Wainwright et al., 2022). At 56 km^2, Coal Creek exhibits an east-west orientation, with north- and south-facing hillslope aspects, and an average slope of 16^o. The characteristics of this catchment have been described previously (Zhi et al., 2020). The land cover is approximately 60 % evergreen forests (e.g., *Picea spp., Abies spp*., *Pinus contorta*) with 10 % montane plants and shrubs (e.g., *Artemisia tridentata*), and 11 % riparian shrubland (dominated by *Salix monticola*). Only 1 % of land is barren. The underlying bedrock is dominated by sedimentary and igneous rock types (including areas of significant mineralization by pyritic ore minerals and associated historic mines). These primarily include sandstone (39 %) and mudstone (15 %) from the Late Cretaceous Mesa Verde formation and Neogene Ohio Creek and Wasatch formations (Manning et al., 2008; Uhlemann et al., 2022). Supplementing these sedimentary units are plutonic rocks (15 %) dominated by granodiorite and quartz monzonite of Oligocene age.

By contrast, the 86 km^2 main stem of the ERP intensive study site is oriented in a northwest-southeast direction, with an average slope 23^o. Land cover within the ERP is more heterogeneous than that of Coal Creek, with extensive regions of barren alpine and subalpine land, mixed forest, including ~10 % deciduous forest (*Populus tremuloides*), ~21 % coverage by coniferous trees (predominantly *Picea engelmannii, and Abies lasiocarpa*), and 27 % intermixed shrub- and grassland meadows. The meadow regions show a mix of perennial bunchgrass (e.g., *Festuca arizonica*), forbs (e.g., *Potentilla gracilis, Veratrum californicum, Lupinus spp.*), and shrubs (*Artemisia tridentata*). Relative to Coal Creek, the East River shows considerable sinuosity, and has an extensive riparian floodplain system dominated by dwarf birch (*Betula grandulosa*) and mountain willow (*Salix spp.*). Plant communities are largely underlain by Cretaceous Mancos shale bedrock (Hubbard et al., 2018), which is entirely absent in Coal Creek, with glacial till also underlying the North Eastern end of the catchment. Agricultural influence is limited to summer grazing of cattle within the ERP.

2.2. Borehole installation: To link export patterns to nitrogen cycling within terrestrial ecosystems, we focused on a montane hillslope within the pumphouse intensive research site at the East River. Five 10-m deep boreholes (0.14 m diameter) were drilled into bedrock along a 137 m-long hillslope-toeslope-floodplain transect. Specific drilling and instrumentation details of these boreholes have been published previously (Wan et al., 2021), however, pertinent here was the installation of porewater samplers, and moisture sensors from the O-horizon, through the weathered saprolite, into the bedrock at >8 m across the transect. Porewater samples were taken throughout the 2017-2019 period, inclusive of two anomalously high- and low-snowpack years.

2.3. Physicochemical measurements: We collected measurements of streamflow and stream water chemistry across a 5-year, 9-month period covering January 1st, 2016 through September 30, 2021. The analysis of the streamflow data has been described recently (Carroll et al., 2021). Stream- and porewater samples were collected for aqueous chemistry measurement using an automatic sampler (Teledyne ISCO 3700, NE, USA) attached to a peristaltic pump. Sampling frequency for stream water samples varied from once per week to three times per week depending on season. Snow was sampled synoptically by digging snow pits and sampling down through the depth of the pit. This depth was dependent on the snow year and varied between 0.4 and 1.6 m. Precipitation samples were also taken synoptically during the monsoonal period, which typically spans the late June to early September timeframe. Prior to anion or cation analysis, water samples were filtered through a 0.45 µm Millipore filter. The anion samples were collected into 2ml polypropylene vials (with no headspace), and the cation samples were collected into high-density polyethylene vials, and acidified with ultra-pure concentrated nitric acid. Anions were measured through ion chromatography (Dionex ICS-2100, Thermo Scientific, USA), and aqueous cation concentration was determined using ICP-MS (Elan DRC II, Perkin Elmer, USA). Dissolved total nitrogen (DTN) was measured on all samples via thermal decomposition and chemiluminescence (Shimadzu TOC-VCSH with the attached TNM-1). Water samples for the determination of ammonium concentrations were taken as described above and measured on a Lachat (QuikChem 8500 series 2 flow injection analysis system).

2.4. Nitrate isotope measurements: The natural abundance of $\delta^{15}N_{NO3}$ and $\delta^{18}O_{NO3}$ in riverine and porewater, snow, and rainfall were measured using the denitrifier method as described previously (Bouskill et al., 2019), and in detail in the supplemental materials. Briefly, samples from either the river (40 ml) or lysimeters (50 - 100 ml) were filtered through a 0.2 µm Sterivex filter and placed on ice in the field. Samples were shipped overnight to Lawrence Berkeley National Laboratory and kept at -80°C until analysis. The isotope ratios of NO_3^- ($\delta^{15}N_{NO3}$ and $\delta^{18}O_{NO3}$), where δ (‰) = (R_{NO3}/ R_{std} -1)*1000, R indicates either $^{15}N/^{14}N$ or $^{18}O/^{16}O$, and 'std' refers to standard reference material, either N_2 in the air for $\delta^{15}N$ or Vienna standard mean ocean water (VSMOW) for $\delta^{18}O$, were measured via the denitrifier method (Casciotti et al., 2002; Sigman et al., 2001). Analysis of the isotopic data is described in detail in supplemental materials. Briefly, we used a simple mixing model to partition the isotopic signal of riverine NO_3^- between atmospheric and soil-derived sources. Furthermore, the change in $\delta^{15}N_{NO3}$ relative to that of $\delta^{18}O_{NO3}$ (i.e., $\Delta\delta^{18}O_{NO3}$: $\Delta\delta^{15}N_{NO3}$) was used in stream and poreater to determine whether a decline in NO_3^- concentrations could be due to source water mixing or due to fractionation mechanisms, as described previously (Granger and Wankel, 2016).

2.5. Analysis of concentration-discharge relationships: Streamwater cQ relationships were initially described using a power law relationship ($c=aQ^b$) for the whole data-set (which was log-transformed prior to analysis), and broken down for each water year (2016-2021). We further calculated the coefficient of variation of solute concentration (CV_c) and discharge (CV_q) (Basu et al., 2011; Knapp et al., 2022; Thompson et al., 2011), using a previously published approach for log-normal data (Knapp et al., 2022),

$$CV = \frac{\sigma}{\mu} = \frac{exp(m_{ln} + 0.5s_{ln}^2)}{exp(2m_{ln} + s_{ln}^2)\,(exp(s_{ln}^2) - 1)} = \sqrt{exp(s_{ln}^2) - 1} \qquad 1$$

where m_{ln} and s_{ln} represent the mean and standard deviation of the data.

2.6. Causality analysis with information theory: To contextualize watershed nitrate export alongside the factors determining transit and loss through the watershed we treat the time series of different hydrological, physical, biogenic, and geogenic data (from 2016 - 2021) as a coupled process network (Ruddell & Kumar, 2009). Herein, the directional impacts from one process (e.g., geogenic leaching, or snowmelt) to the other (e.g., nitrate export) is be quantitatively inferred by Shannon information entropy (*H*) and its transfer (TE) (unit bits).

$$H = -\sum_{i=1}^{n} p\,(X_i) log_2 p(X_i) \qquad 2$$

$$T_{X->Y} = \sum_{y_i, y_{i-1}, x_{i-j}} p\left(y_i, y_{i-1}, x_{i-j}\right) log_2 \frac{p\left(y_i | y_{i-1}, x_{i-j}\right)}{p(y_i | y_{i-1})} \qquad 3$$

where $p(x)$ is probability density function (PDF) of x, $p(y_i, y_{i-1}, x_{i-j})$ is the joint PDF of current time step y_i, previous time step of y_i, and jth time step before of x_i. $p(y_i|y_{i-1}, x_{i-j})$ and $p(y_i|y_{i-1})$ denote conditional PDF of the corresponding variables. For example, the information entropy transfer from snowmelt to nitrate export is calculated as Shannon entropy reduction (uncertainty reduction) of present nitrate export given the historical snowmelt records (up to12 month time lags) and excluded the influence from the previous time step for nitrate export. In order to ensure the calculated transfer entropy does not stem from randomness, we conduct statistical significance tests by first randomly shuffling the time series 10 times to obtain a distribution of transfer entropy assuming the random shuffle will break the causality between SWE and NO_3^{EXPORT}. Then a significance threshold of $TE^{SWE} -> NO_3^{EXPORT}$ is determined by the 95%

confidence threshold of the shuffled transfer entropy (Yuan et al., 2022). We report causality only when the $TE^{SWE} \rightarrow NO_3^{EXPORT}$ of the original time series data is larger than its significance threshold. We applied this causality modeling approach to the observed time series of watershed variables at both the Coal Creek and ERP. The factors included in the analysis were chosen as proxies for the different sources contributing stream NO_3^-, and included biogenic solutes derived from shallower soils (e.g., DOC), or deeper bedrock derived solutes (e.g., Mg), redox active compounds (e.g., SO_4^{2-}), and hydrological variables influencing nutrient flux and riverine turnover (e.g., SWE and water temperature). Their relevance to NO_3^- was visualized in a network (Bastian et al., 2009) from which quantitative associations between different variables can be identified.

2.7. Assessment of annual and snowmelt nitrate export: We calculated a time-series of total mass exports leaving the Coal Creek and ERP catchments *Ex(t)* (Mg/year) using the discharge *Qs(t)* and concentration *Cn(t)* time series by integrating from day 1 of each water year to day 365 for annual time series, and during the specific time periods related to snowmelt (Equation 4). The mass export is the multiplication of discharge *Qs(t)* (m^3/s) and concentration of nitrate *Cn(t)* (mg-N/L converted to kg/m^3) and summed for all daily time steps (dt):

$$Export = Ex(t) = \sum_{day\ 1}^{day\ 365} Qs(t)Cn(t)dt \qquad 4$$

Discharge and concentration time series were gap-filled and interpolated using an averaging method when missing values exist. N exports (Mg/year) were converted to N yields by dividing by the area of each catchment and converting mass from Mg to kg to match the units of atmospheric deposition (kg/hectare/year). We relate solute fluxes from inputs (e.g., atmospheric deposition) to the riverine outputs through equation 5 which describes the retention of N within each watershed on a water year basis:

$$Retention\ Capacity = Ret\% = \frac{Deposition - Yields}{Deposition} * 100 \qquad 5$$

In addition to input from atmospheric sources we also evaluate the potential contributions to NO_3^- export from bedrock weathering within the ERP. Correcting the estimated annual NO_3^- flux from the Mancos Shale saprolite of (Wan et al., 2021) with improved flow rates (Tokunaga et al., 2022) results in 2.0 kg ha^{-1} yr^{-1} from the critical zone of a hillslope to the floodplain. Only a fraction of this hillslope value is likely to reach the river due to denitrification while traversing the floodplain. Furthermore, this value is unlikely to be representative of the watershed scale hillslope weathering flux as parts of the watershed is underlain by glacial till, not shale, while infiltration within north facing slopes (where these initial measurements were made) is higher than south-facing slopes, promoting higher rates of weathering. For these reasons, we assume a smaller range (0-1 kg ha^{-1} yr^{-1}) of NO_3^- derived from shale weathering likely contributes to the catchment NO_3^- export.

3. Results

3.1. Concentration-discharge relationships: The time span of this study covered both historical highs and lows of snow water equivalence (SWE, m) and discharge (Q, m s^{-1}) within Coal Creek and ERP. Both 2017 and 2019 were above average snowpack depth and discharge, while 2018 represented a historic low. Figure 2 provides the time course of SWE for the East River Watershed, and Q for the specific regions. While the temporal trends in snowmelt driven discharge were the same between Coal Creek and ERP, the larger drainage area and lower proportion of forest coverage means that the streamflow was much higher within the ERP.

Figure 2: Discharge, and snow water equivalent throughout the study period (2016-2021). River discharge (m s^{-1}) data depicts both the Coal Creek and ERP catchments. Snow water equivalent (m) is derived from the SNOTEL station (Site 380).

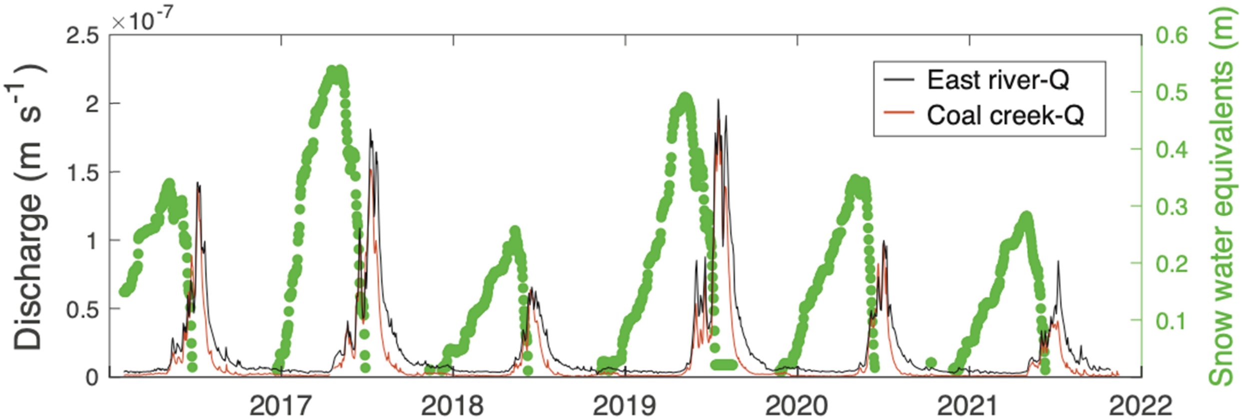

The magnitude of the annual average NO_3^- export, after accounting for catchment areal extent (Eq. 4 & 5), was higher within the ERP (1.71 Mg ± 1.2) relative to Coal Creek (0.3 Mg ± 0.13) (Table 1 & Fig. S2). The pulse-shunt associated with snowmelt is responsible for the bulk of solute export, accounting for 80-90% and 50-90 % of total NO_3^- export in both Coal Creek and ERP, respectively. The riverine NO_3^- concentrations spanned a similar order of magnitude within both the Coal Creek and ERP (Fig. 3a), and exhibited an overall chemostatic relationship with discharge, showing minimal fluctuation under increasing discharge. However, slight differences in cQ for NO_3^- between Coal Creek and ERP are noted at intermediate discharge, whereby export at ERP is slightly diluted, while Coal Creek is concentrated (Fig. 3a, i). The trends in CV_c/CV_q support the highly variable nature of the cQ data for NO_3^- (Fig. 3b), however, using this approach, both catchments show evidence of chemodynamic behavior ($CV_c/CV_q > 1$). When considered as independent water years (2016 - 2021), Coal Creek shows more conservative behavior, with two years of overall chemostasis and the remainder chemodynamic. The strongest chemodynamic regimes occur during the driest years (2018 and 2020). The CV_c/CV_q for the ERP showed stronger positive chemodynamic behavior across multiple years relative to Coal Creek, in contrast to the cQ data. For both Coal Creek and ERP, this analysis shows the importance of heterogeneous sources contributing to the aggregate export signal at different times of the year.

Table 1: Annual nitrate export magnitudes between East River and Coal Creek. These calculations use gap-filled data, and are expressed as a function of the size of each watershed. Annual NO_3^- flux (Mg-megagrams) is calculated from Equation 4 at the water year time scale. Q yield (km^3) is the total volume of water that exited the watershed for each water year. Atm. NO_3^- deposition (Mg) is the total (i.e., wet + dry) nitrate deposition (kg-N/ha), summed across each watershed area.

		2016	2017	2018	2019	2020	2021
East River	Annual NO_3^- export (Mg)	3.8	1.1	0.6	2.8	1.2	1.2
	Q Yield (km^3)	0.05	0.07	0.03	0.09	0.04	0.03
	Atm. NO_3^- deposition (Mg)	8.6	9.1	7.3	6.4	7.3	8.4
Coal Creek	NO_3^- annual export (Mg)	0.3	0.3	0.1	0.5	0.3	0.3
	Q Yield (km^3)	0.02	0.03	0.01	0.03	0.02	0.01
	Atm. NO_3^- deposition (Mg)	6.4	6.5	5.3	4.9	5.3	6.1

Figure 3: (a) Concentration-discharge relationships for different solutes within the ERP and Coal Creek catchments (i) nitrate, (ii) dissolved total nitrogen, (iii) chloride, and (iv) magnesium. Also shown are the lines of best fit, the slope of which is represented in the powerlaw relationship as exponent *b* ($c=aQ^b$). (b) The ratio between the coefficient of variation for solute concentration and discharge (CV_c/CV_q) plotted against the exponent (*b*) of the powerlaw relationship for the same solutes as in (a). Each plot depicts the entirety of the data for the two watersheds (larger points with solid black outline) and the data for each water year. Also depicted in these plots are the positive and negative linear relationship between CV_c/CV_q and *b* (solid black lines), and the threshold point (at $CV_c/CV_q = 0.5$, dotted line) separating chemostatic from chemodynamic regimes.

Distinct relationships emerge during the rising and falling limb (Fig. 4, & Table 2). The rising limb has little impact on riverine NO_3^- in either the ERP ($b = 0.05$), or Coal Creek ($b = 0.1$). However, the falling limb of the snowmelt period flushes NO_3^- into the ERP ($b = -0.6$), as the groundwater table reaches into the shallower soils. This impact is much weaker in Coal Creek (*b* = -0.06). `

Figure 4: Relationship between the concentration of different nitrogen species (NO_3^-, DON), chloride, and magnesium, relative to the discharge for (a) the East River catchment, and (b) Coal Creek. The hydrograph is divided into the rising limb (increasing during the annual snowmelt period), and the falling limb (decreasing to baseflow).

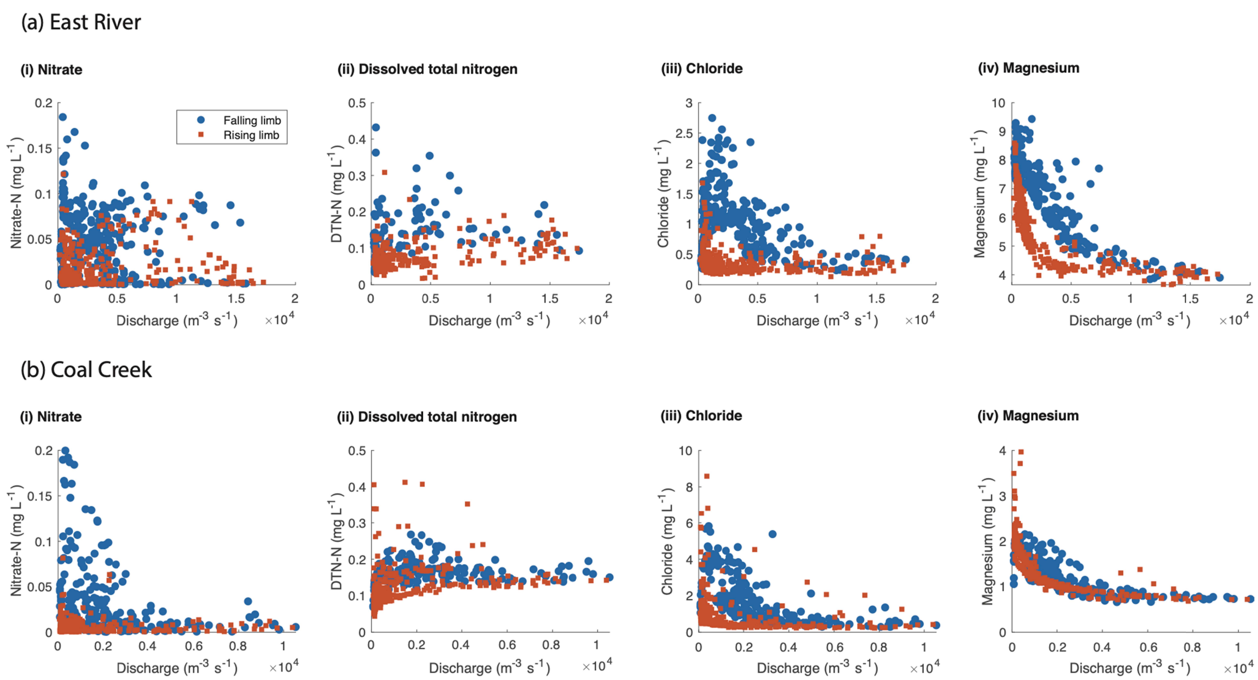

DTN showed a different relationship with Q than NO_3^-, which, given that riverine NH_4^+ was extremely low (generally non-detectable, and always < 1 μM), likely reflects the export of dissolved organic nitrogen in these systems. Within both catchments, DTN export increased with increasing Q (Fig. 3a), which was stronger in Coal Creek (*b* = 0.16) relative to ERP (*b* = 0.07). This relationship was also apparent under the falling limb in the ERP, and under increasing and decreasing Q in Coal Creek (Table 2). The CV_c/CV_q ratio was typically low (<0.5) for both Coal Creek and the ERP, indicating that the variability in DTN export is strongly related to the variation in discharge.

Table 2: Exponent *b* for the concentration-discharge of various elements. The table provides the value calculated from the complete dataset. In brackets are the ranges in *b* spanned by individual

years (2016 - 2021), followed by the *b* values during the rising limb and the falling limb of the hydrograph.

	East River	Coal Creek
Nitrate	0.013 (-0.06/ 0.38| 0.05/ -0.6)	-0.01 (-0.23/ -0.2| 0.1/ -0.06)
Dissolved total nitrogen	0.07 (-0.02/ 0.37| 0.16/ 0.08)	0.16 (0.11/ 0.2| 0.14/ 0.2)
Chloride	-0.02 (-0.08/ 0.19| -0.03/ -0.5)	-0.07 (-0.3/ 0.12| -0.11/ -0.3)
Magnesium	-0.14 (-0.18/ 0| -0.15/ -0.24)	-0.26 (-0.3/ -0.21| -0.17/ 0.25)

Chloride export was measured as a conservative tracer of watershed export processes, and showed a broad chemostatic relationship with Q in ERP (b = -0.02, with an interannual range = -0.08 - 0.19), and a slightly stronger dilution of Cl concentration within increasing Q in Coal Creek (b = -0.07, interannual range = -0.3 - 0.12) and ERP. The cQ relationship for magnesium provides insight into the export behavior of a predominantly bedrock-derived solute. Riverine Mg concentration was far higher in the ERP where soils are underlain by a Cretaceous Mancos shale bedrock, however, the trajectory of Mg export was similar between the catchments and generally showed a non-linear decline in concentration under increasing Q (Fig. 3a, 4). CV_c/CV_q ratios generally underlie the observations from cQ slopes, with groundwater, and geogenically-derived solutes showing little variability in concentrations, and are strongly driven by changes in discharge (Fox et al., 2022).

Causality analyses (performed using transfer entropy, (Ruddell & Kumar, 2009) was used to further parse out the factors regulating NO_3^- transit and export (Fig. S3a/b). SWE and water temperature were important factors governing NO_3^- export from both catchments (Fig. S3c). However, both biogenic and geogenic variables were closely associated with NO_3^- release to streams within the ERP, indicating the contribution of both shallow and deep sources to the NO_3^- aggregate flux. By contrast, NO_3^- exported from Coal Creek showed no direct connection to biogenic or geogenic export (Fig. S3c), indicating the strong role atmospheric deposition plays in contributing to NO_3^- export.

3.2. Streamwater $\delta^{15}N_{NO3}$ and $\delta^{18}O_{NO3}$: The isotopic composition of NO_3^- ($\delta^{15}N_{NO3}$ and $\delta^{18}O_{NO3}$) in stream water within Coal Creek and the ERP was measured across a two-year period between 2019 to 2021, capturing historic highs and lows in snowpack depth and streamflow (Fig. 5a). The lower NO_3^- concentrations within Coal Creek (< 2 µM) precluded isotopic measurements during much of the baseflow period, and measurements focused mainly on the snowmelt period (Fig. 5a). The $\delta^{15}N_{NO3}$ within the ERP showed a narrower range of values than Coal Creek. In the ERP $\delta^{15}N_{NO3}$ spanned -2.3 - 19.2 ‰ (3.8 ± 4.4 ‰, mean and standard deviation), and 1.4 - 24 ‰ (8.9 ± 6 ‰) in Coal Creek. Similarly, $\delta^{18}O_{NO3}$ ranged from 1.2 to 27.8 ‰ (11.8 ± 6.8 ‰) in the ERP, and 1.5 - 44.5 ‰ (19.3 ± 7.3 ‰) in Coal Creek (Fig. 5b).

Figure 5: River concentration and isotope data for the (a) ERP, and (b) Coal Creek. Subplots a and b are divided into three panels, depicting the river nitrate concentrations (top panel), $^{15}N_{NO3}$ (middle panel), and $^{18}O_{NO3}$ (bottom panel). Panel (c) depicts the relationships between $^{15}N_{NO3}/^{18}O_{NO3}$ within streamwater collected within Coal Creek and the ERP.

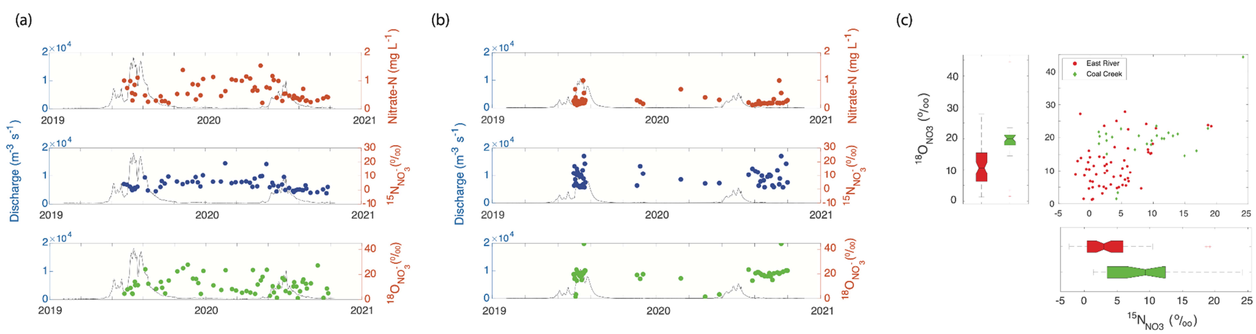

3.3. Sources of exported nitrate: We used a simple two-end member mixing model to determine the contributions of atmospheric and soil-/ saprolite-derived NO_3^- to aggregate NO_3^- export. The atmospheric component of this mixing model was derived from measurements of the isotopic composition of precipitation from both Coal Creek and ERP. The isotopic signal of both snow and rainfall overlapped between the two catchments, showing an average (± standard deviation) $\delta^{15}N_{NO3}$ of 6.4 ± 4.3 ‰ and 18.6 ± 5 ‰ and a $\delta^{18}O_{NO3}$ average of 73 ± 11.1 ‰ and 65.6 ± 9.6 ‰, for rainfall and snowfall respectively (Fig. S4). The soil-derived signal is attributable to nitrification, and is calculated from a $\delta^{18}O$ value of O_2, and measured values of $\delta^{18}O$ for porewater from the hillslope boreholes. The specific approach for estimating the $\delta^{18}O$ values of nitrification can be found in the supplemental material and methods. Measurements of dissolved

NO_3^- were not made for Coal Creek soils, so mixing model calculations were made using nitrification data derived from ERP soils, which overlap with previously published values (Granger & Wankel, 2016). This mixing model demonstrated that a larger fraction of riverine NO_3^- exported from Coal Creek was derived directly from atmospheric deposition (~41 %), with the remainder sourced from soil pools. The range of atmospheric contributions to NO_3^- export in Coal Creek varied from 20 to 62 % (Table S1). A weighted approach to calculating percent contribution of atmospheric sources to distinct periods of the hydrograph shows it to be larger during the snowmelt period (34 ± 5 %) relative to baseflow (20 ± 4 %) (Table S2). By contrast, the majority of exported NO_3^- from the ERP was derived from nitrification (~82 %), with a smaller direct contribution from atmospheric NO_3^- deposition, ranging across the year from 16 to 29 %. A biplot depicting $\delta^{18}O_{NO3}$ and $\delta^{15}N_{NO3}$ suggests that the groundwater accumulating within toeslopes, and from NO_3^- the floodplain were significant sources of ERP riverine NO_3^- (Fig. S4). Finally, the ERP showed a relatively high range of $\delta^{18}O_{NO3}$ throughout the year, however, the percent contribution of atmospheric NO_3^- to export was similar during the snowmelt period (22 ± 3 %), and baseflow (24 ± 7 %) (Table S2).

Periodically, the NO_3^- isotope time series within ERP showed concomitant enrichment of both $\Delta\delta^{18}O_{NO3}$: $\Delta\delta^{15}N_{NO3}$ (Fig. 5a, c). These periods occur during snowmelt and under baseflow conditions, albeit with slightly different enrichment relationships between the two isotopes, of 1.2 and 0.6 during snowmelt and baseflow respectively (Fig. S5). These periods suggest an actively fractionating mechanism (e.g., denitrification) is contributing to NO_3^- loss from solution. By contrast, evidence for strongly fractionating loss pathways within Coal Creek were not observed.

3.4. Terrestrial nitrate cycling in the East River: To strengthen our understanding of how different sources and sinks contribute to the aggregate NO_3^- export within the ERP catchment, we developed a depth-resolved, time series of $\delta^{15}N_{NO3}$ and $\delta^{18}O_{NO3}$ across a hillslope-toeslope-floodplain transect. This time series permits the identification of major source-sink hotspots across the terrestrial system that likely account for the stronger biogeochemical processing of nitrogen within the ERP. Moreover, the time period of intensive sampling encompassed the same event driven trajectory as the riverine data, capturing historic high and low snowpack depths, which dictated much of the variance in water table depth, and runoff. Across this transect, the $\delta^{15}N_{NO3}$ and $\delta^{18}O_{NO3}$ spanned a large range indicative of multiple sources contributing to nitrate accumulation and cycling (Fig. 6a, S6a). Within shallower soil horizons, $\delta^{15}N_{NO3}$ and $\delta^{18}O_{NO3}$ ranged from -7.5 to 19 ‰ and -10.5 to 21 ‰, respectively. Within the shale weathering zone $\delta^{15}N_{NO3}$ ranged from ~ 1 ‰ to 20 ‰, and $\delta^{18}O_{NO3}$ from -10 ‰ to 14 ‰. The fractured bedrock showed a range in $\delta^{15}N_{NO3}$ from ~ -5 ‰ to 8 ‰, and -29 ‰ to 22 ‰ for $\delta^{18}O_{NO3}$.

A simple mixing model was used to calculate the contribution of atmospheric deposition to subsurface NO_3^- pools across depth and time. Broadly, percent atmospheric NO_3^- increased with depth from 12 % (range: 1.1 - 41 %) within shallow soil layers to 20.2 % (0 - 43.4 %) within the fractured bedrock, with the saprolite weathering zone showing intermediate levels of atmospheric NO_3^- (~14 %: 4 - 33 %. Table S1, Fig. S6a). Contribution of atmospheric NO_3^- to NO_3^- pools increased during the snowmelt period (Fig. S6b) within the shallow soils, but particularly in saprolite weathering zone, where the contribution increased to ~21 %, with an upper range of ~32%. This contribution dropped under baseflow conditions (~9 %).

The trajectory of the $\Delta\delta^{18}O_{NO3}$: $\Delta\delta^{15}N_{NO3}$ showed distinct relationships across the different regions of the soil profile (Fig. 6b). The shallow soil horizon showed a weak relationship between $\Delta\delta^{18}O_{NO3}$: $\Delta\delta^{15}N_{NO3}$ of ~ 0.06. However, both the weathering zone and the fractured bedrock showed stronger $\Delta\delta^{18}O_{NO3}$: $\Delta\delta^{15}N_{NO3}$ relationships of ~ 0.7 and 0.5, respectively. The weathering zone, which shows the strongest $\Delta\delta^{18}O_{NO3}$: $\Delta\delta^{15}N_{NO3}$ trajectory, shows a clear combination of both mixing processes, and fractionating processes (e.g., nitrate reduction, nitrate reoxidation). However, approximately 25 - 30 % of the nitrate in weathering zone originated from atmospheric deposition (which imparts a high $\delta^{18}O_{NO3}$ value), precluding the identification of any one process dominating NO_3^- dynamics and demonstrating this zone to be a strong integrator of different NO_3^- sources.

Figure 6: Relationships between $^{15}N_{NO3}/^{18}O_{NO3}$ within the terrestrial zone, (a) $^{15}N_{NO3}/^{18}O_{NO3}$ across different soil depths on the hillslope (i.e., Shallow soil horizon, weathering zone, and consolidated bedrock). The correlation between the $^{15}N_{NO3}/^{18}O_{NO}$ measurements are provided in brackets in each legend. (b) The same relationship within two different depths (i.e., shallow soil horizon, and saprolite weathering zone,) at different points along the transect encompassing the upper- and mid-hillslope, and the toeslope. As for panel a, the value in brackets represents the correlation between the $^{15}N_{NO3}/^{18}O_{NO}$.

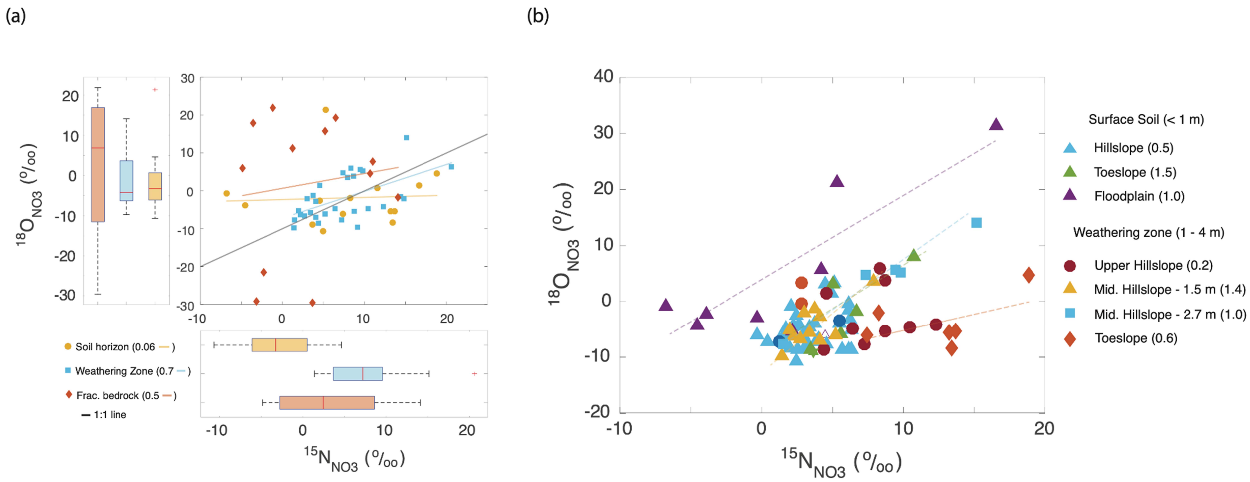

The $\Delta\delta^{18}O_{NO3}$: $\Delta\delta^{15}N_{NO3}$ relationship also showed clear variability across the hillslope-toeslope-floodplain transect that was related to water residence time. Regions with long transit times, i.e., within shallower soils at the floodplain, and the weathering zone (~2.7 m depth) at the hillslope, showed a concomitant enrichment between $\Delta\delta^{18}O_{NO3}$: $\Delta\delta^{15}N_{NO3}$ (Fig. 6b), which is indicative of an actively fractionating mechanism (e.g., denitrification). The shallow soils at the toeslope, and the soil-saprolite transition zone at the mid-hillslope (~1 m) had a slightly higher relationship between $\Delta\delta^{18}O_{NO3}$: $\Delta\delta^{15}N_{NO3}$ of 1.5. Finally, the regions with slightly faster transit times, i.e., shallow soils on the hillslope where soil moisture increases briefly with snowmelt as the water table rise, or the weathering zone of the toeslope, both show a lower $\Delta\delta^{18}O_{NO3}$: $\Delta\delta^{15}N_{NO3}$ ratio of 0.6, which implies both source water mixing and *in situ* transformation occurs in this region.

4. Discussion

Gradients in vegetation, topography, geology, and geomorphology all play critical roles in determining nitrogen availability, and regulating its retention and release from mountainous headwaters (Bormann & Likens, 1967; Sebestyen et al., 2014, 2019). Paired catchment studies are important approaches to improve understanding of the role distinct geophysical and ecological traits play in the transformation of nitrogen while controlling for climatic properties, and the magnitude of nitrogen deposition.

When normalized to catchment area, the East River at pumphouse (ERP) exported between 3 to 12x as much NO_3^- as Coal Creek (Table 1 & Fig. 8). The ERP is the larger catchment and nitrate deposition is calculated to be a little higher (7.8 ± 1 MG in ERP, relative to 5.7 ± 0.7 MG in Coal Creek). Both catchments show large variability in NO_3^- concentrations across the measured range in discharge (Fig. 3a/b), indicating the contribution of multiple sources of terrestrial NO_3^- to the aggregate downstream export profile (Thompson et al., 2011). A causality analysis illustrates both similarities in the main factors driving NO_3^- export between the two catchments (e.g., the considerable influence of SWE), but also clear distinctions. For example, NO_3^- export in the ERP is more strongly related to biogenic (e.g., microbial turnover of DOC, which can be tied to NO_3^- reduction) and geogenic (e.g., bedrock weathering) processes (Fig. S3), implying a more complex role of shallow and deep sources of NO_3^- in the ERP (Zhi & Li, 2020). By contrast, nitrate export in Coal Creek showed little information transfer between biogenic and geogenic processes, suggesting little microbial transformation prior to export, and no contribtion of bedrock weathering to NO_3^- export. In the following sections we discuss the role of vegetation, redox heterogeneity, and bedrock properties in contributing to differences in the retention and release of NO_3^- between the two catchments.

Figure 7: Schematic representation of different retention of NO_3^- (in megagrams, MG) across the two catchments as a function of their distinct vegetation and bedrock properties. Also provided are the direct contribution of atmospherically deposited nitrate ($N^{18}O_3^{ATM}$) to exported NO_3^-, and the % of atmospherically deposited NO_3^- retained in different watersheds. Estimates of the contribution of bedrock weathering are also provided for ERP. The units for the different fluxes are in megagrams (MG), and are normalized to the individual catchment size.

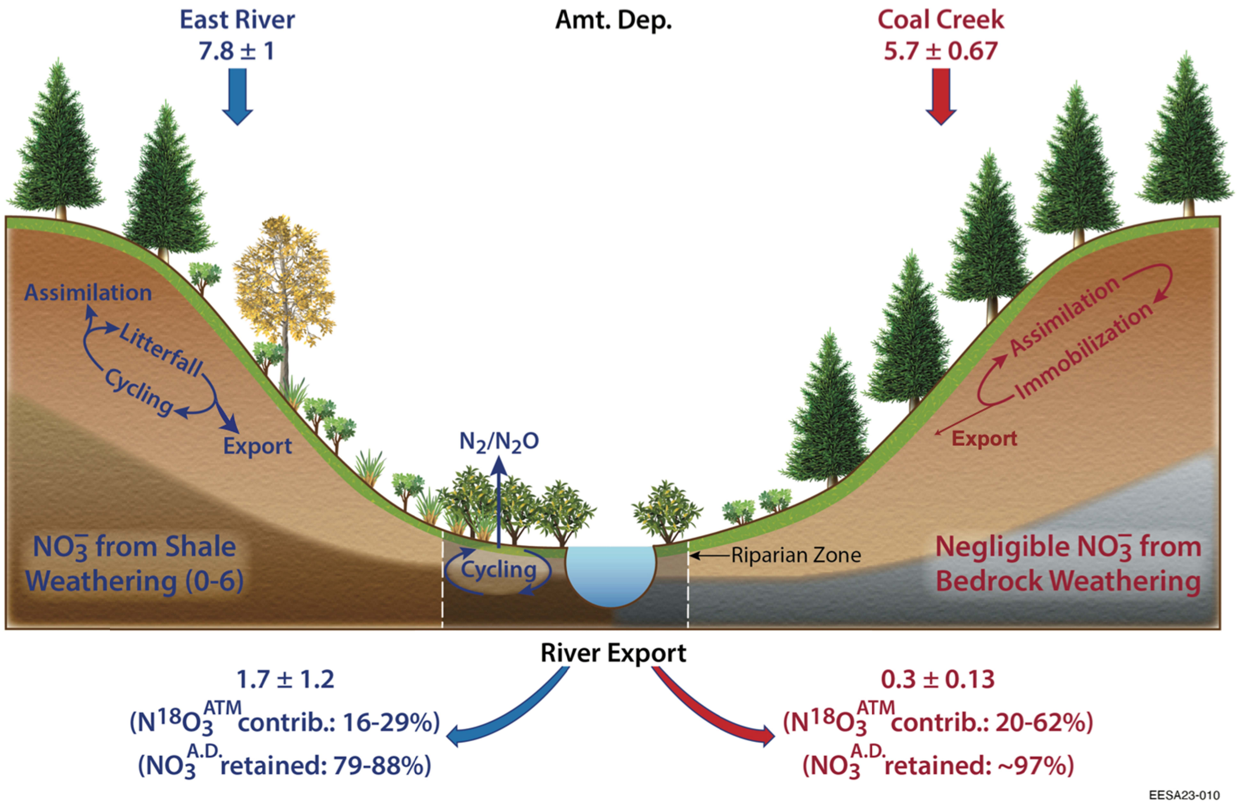

4.1. Vegetation controls on NO_3^- cycling: The contrasting vegetation distributions between Coal Creek and ERP likely play a large role in the retention and release of NO_3^- at the catchment scale. Coal Creek is dominated by coniferous forests (predominantly *Picea engelmannii* and *Abies lasiocarpa*), while ERP has a more heterogeneous land cover, with extensive regions of barren alpine and subalpine land, mixed forest, and shrub and grassland. The strong forest coverage of Coal Creek can give rise to efficient and closed nitrogen cycles (Fahey et al., 1985; Gosz, 1981), where the turnover (depolymerization and mineralization) of soil nitrogen pools, and recycling of internal pools sustains nitrogen demand, and reduces NO_3^- export from the catchment (Fig. 8). Moreover, plant traits associated with conifers, including a higher leaf mass area and lower nitrogen content in litter, would further nitrogen turnover and loss. Further supporting this idea of higher retention in forested catchments, a recent study (Gurmesa et al., 2022) demonstrated strong assimilation of NO_3^-, relative to NH_4^+, by plants on a global scale, contrary to expectations for inorganic nitrogen assimilation based upon the energetic costs of assimilating reduced compounds (Kronzucker et al., 1997). Furthermore, low NO_3^- concentrations within Coal Creek (Table 1 & Fig. 8) may stem from immobilization of nitrogen by bacteria and fungi during the decomposition of woody debris following tree mortality. Previous studies have attributed the net retention in forested watersheds, and subsequent declines in NO_3^- export, to the accumulation of high C: N woody debris, and immobilization of dissolved nitrogen (Lajtha, 2020). Preliminary work has shown a higher mortality rate amongst conifers within Coal Creek relative to the ERP (Falco et al., in prep.), which could contribute to the disparity in retention between the two catchments.

The vegetation in ERP includes montane species (e.g., *Artemisia spp.* and *Festuca spp.*), Aspen glades (*Populus tremuloides*), and conifer stands (*Picea engelmannii, and Abies lasiocarpa*), that likely lead to a more open nitrogen cycle, particularly through litter accumulation and turnover (Maavara et al., 2021). The difference in vegetation communities between the two catchments also contributes to distinct hydrological cycles, which play a critical role in nitrogen cycling and solute export (Webb et al., 2020; Woelber et al., 2018). The dense forest coverage within Coal Creek increases the loss of snow via canopy interception, ablation, and evapotranspiration, reducing that contributing to river flow (Fig. 2) (Sprenger et al., 2022). A higher rate of ET can lower the depth of the groundwater table (Condon et al., 2020), reducing connectivity between hillslopes and the river, increasing nitrogen retention in upslope regions of Coal Creek.

4.2. Bedrock properties and nitrogen cycling: A further fundamental difference between Coal Creek and ERP concerns the underlying bedrock. The ERP is largely underlain by nitrogen-rich Mancos Shale bedrock, which has been previously reported to show high rates of weathering as snowmelt-driven groundwaters rise and fall (Wan et al., 2019, 2020; Winnick et al., 2017). Wan et al., (Wan et al., 2020) estimated a base cation weathering rate for a hillslope within the ERP of 55.3 ± 4 Kmol$_c$ ha^{-1} yr^{-1}, and a shale-nitrogen release rate of 18.9 ± 4.4 kg ha^{-1} yr^{-1}, and a specific hillslope NO_3^- export of ~2.0 kg ha^{-1} yr^{-1}. The bulk of this exported NO_3^- is likely assimilated by plants or reduced by microbes within the floodplain (see discussion below), therefore, the contribution of geogenic sources of NO_3^- to the aggregate export signal remains uncertain. Water table depths dominate solute transport to the river, and shape the characteristic cQ relationships for different solutes. Zhi et al., formally described how distinct solute sources govern water chemistry within Coal Creek, demonstrating that low water table depths under baseflow conditions, or during particularly dry years, activate organic-poor, geogenic sources of solutes

(Zhi et al., 2019). The relationship between Mg and discharge replicates this dilution pattern within both catchments (Fig. 3a,b). However, NO_3^- demonstrates strong variability with stream discharge (Fig. 3a). Incidences of high NO_3^- export under baseflow conditions could represent the contribution of geogenic sources in the ERP, however, the variability in cQ is similar to that in Coal Creek (Fig. 3a, b), which is underlain by crystalline igneous rocks containing only trace amounts of nitrogen Holloway & Dahlgren, 2002). The high NO_3^- concentrations exported under low discharge in both catchments likely reflects the legacy storage, and subsequent mobilization, of groundwater NO_3^- (Johnson & Stets, 2020), which is contributed to by bedrock weathering in the ERP (Wan et al., 2020).

Estimating the contribution of bedrock NO_3^- to exports is further complicated by the variability in the extent of bedrock weathering (and nitrogen release) throughout the ERP catchment, particularly with aspect and the degree of infiltration (Pelletier et al., 2018). The northeast-facing hillslope, where the bulk of our data is derived, shows high fracture density and a high weathering rate. There is, however, considerable variability in the weathering potential of the Mancos shale throughout the ERP, with areas towards the headwaters of the catchment underlain by older, harder shale, with fewer fractures through the shale (discussed further in Maavara et al., 2021). We therefore consider that at the catchment scale, bedrock nitrogen from the hillslope contributes significantly less to watershed NO_3^- export than it likely does to floodplain nitrogen cycling, and, as such, assume a value between 0 - 1 kg ha^{-1} yr^{-1} for our estimate of catchment export (Fig. 8). After accounting for this potential contribution of bedrock weathering to NO_3^- export, Coal Creek shows a significantly higher retention of NO_3^- relative to the ERP. We estimate that approximately 97 % of deposited NO_3^- is retained in Coal Creek, relative to ~78-88 % in the ERP.

4.3. Riparian contributions to NO_3^- retention: Coal Creek and the ERP differ further in geomorphology, with the ERP showing much higher sinuosity through the valley and a larger areal extent of the riparian region. These are important features regulating the sources of exported NO_3^-. The majority of NO_3^- exported by watersheds tends to be derived close to the river (Sebestyen et al., 2019). A smaller riparian region within Coal Creek reduces preprocessing of that NO_3^- prior to export, which might account for the higher contribution of atmospheric sources of NO_3^- to aggregate export (Fig. 5). This contribution increases during the snowmelt period (Table S2), consistent with previous analyses partitioning contributions to aggregate NO_3^- export (Sebestyen et al., 2019), and likely attributable to rapid transit times, and fewer opportunities for biological transformations during the snowmelt period.

The ERP shows a higher variability in the sources of NO_3^- contributing to its aggregate export (Fig. 5a). The mobilization of soil-derived NO_3^- during snowmelt results in a chemodynamic relationship with streamflow (Fig. 3b), and increasing export under the rising and falling limb of snowmelt (Fig. 4a). Across the year, the exported NO_3^- has a distinct isotopic composition from the terrestrial sources. For example, the contribution of atmospheric NO_3^- to terrestrial pools shows a strong interannual pattern, increasing during the snowmelt period, and declining during baseflow (Fig. S6b). This pattern is not reflected in the river NO_3^- isotopic signal (Fig. 5a, & Table S2), reflecting the contribution of different ecosystem control points, particularly, the overriding impact of critical zone and floodplain processes. The fluctuating water table also prolongs transit times and reactivity within the critical zone, and the riparian region. This promotes the formation of strong oxic/anoxic gradients, and the spatial and temporal coupling of aerobic (e.g., nitrifying) and anaerobic (denitrifying) metabolisms (Bouskill et al., 2019). A mass balance calculation using subsurface NO_3^- cQ from the upper hillslope region to the toeslope suggests that much of the NO_3^- accumulating within the hillslope critical zone is subject to denitrification prior to export (Wan et al., 2020). Further support for this mechanism of loss comes from our observations of very low to undetectable NO_3^- concentrations within riparian regions in ERP and the isotopic enrichment of NO_3^- (Fig. S4), along a $\Delta\delta^{18}O_{NO3}$: $\Delta\delta^{15}N_{NO3}$ trajectory of 0.6 (Fig. 7), indicative of actively fractionating mechanisms (e.g., nitrite oxidation and denitrification, Granger & Wankel, 2016).

The functional potential for denitrification was observed across the ERP riparian region (Carnevali et al., 2020), however, this area was also been shown to be a potential hotspot for DNRA (Carnevali et al., 2020), which fractionates the ^{15}N and ^{18}O of NO_3^- in a similar manner ($^{15}\varepsilon$:$^{18}\varepsilon$ = 0.5 - 1.0) to denitrifying bacteria (Asamoto et al., 2021). Rogers et al., modeled the hydrological and biogeochemical processes retaining and releasing nitrogen within the ERP riparian region, concluding that these regions are major control points for river corridors, providing ~20 % of the stream NO_3^-, but remaining major sinks for NO_3^- , due to a combination of denitrification and dissimilatory nitrate reduction to ammonium (DNRA) (Rogers et al., 2021). Under certain conditions, DNRA and denitrification co-exist (Jia et al., 2020), however, their environmental impact is distinct. At the ecosystem scale DNRA tends to function as an ecosystem retention mechanism for nitrogen, which might be important in nitrogen limited ecosystems.

5. Conclusions

Nitrogen retention plays a critical role in ecosystem function in mountainous watersheds. However, the nitrogen cycle is undergoing substantial perturbation (Steffen et al., 2015), and the reported onset of oligotrophication of the nitrogen cycle in undisturbed catchments (Craine et al., 2018; Mason et al., 2022), can undermine watershed function under future warmer and drier climate scenarios predicted to disturb mountainous ecosystems (Siirila-Woodburn et al., 2021). Predicting how this disturbance might feedback onto watershed function can be improved by viewing function through the lens of watershed traits (McDonnell et al., 2007), which is emphasized by the current paired catchment approach. Watershed traits, including topography, bedrock weathering properties, soil properties, land cover, etc., are emergent features of the historical climate, and regulate the storage and release of water and solutes between different catchments. Improving our understanding of whether analagous assemblages of traits retain and release solutes in comparable ways (i.e., whether conifer dominated forests through the Rocky Mountains retain atmospheric nitrate and release a larger share of unprocessed nitrate) would allow these catchments, and their potential response to disturbance, to be considered together in regional scale models. This study also demonstrates the importance of integrating common measurements, such as cQ analysis, with stable isotope measurements of NO_3^-, to improve understanding of how catchments with similar cQ relationships can differ strongly in their nitrogen cycles.

Acknowledgements: This material is based upon work as part of the Watershed Function Scientific Focus Area supported by the U.S. Department of Energy, Office of Science, Office of Biological and Environmental Research under contract number DE-AC02-05CH11231.

Data availability: The data and scripts used to produce the figures are available publicly through https://data.ess-dive.lbl.gov/data via doi:10.15485/1660462, doi:10.15485/1660456. While streamflow and discharge data are available at doi:10.15485/1779721, and doi:10.21952/WTR/1495380.

References

Alexander, R. B., Boyer, E. W., Smith, R. A., Schwarz, G. E., & Moore, R. B. (2007). The Role of Headwater Streams in Downstream Water Quality1: The Role of Headwater Streams in Downstream Water Quality. *JAWRA Journal of the American Water Resources Association*, *43*(1), 41–59. https://doi.org/10.1111/j.1752-1688.2007.00005.x

Asamoto, C. K., Rempfert, K. R., Luu, V. H., Younkin, A. D., & Kopf, S. H. (2021). Enzyme-Specific Coupling of Oxygen and Nitrogen Isotope Fractionation of the Nap and Nar Nitrate Reductases. *Environmental Science & Technology*, *55*(8), 5537–5546. https://doi.org/10.1021/acs.est.0c07816

Ascott, M. J., Gooddy, D. C., Wang, L., Stuart, M. E., Lewis, M. A., Ward, R. S., & Binley, A. M. (2017). Global patterns of nitrate storage in the vadose zone. *Nature Communications*, *8*(1), 1416. https://doi.org/10.1038/s41467-017-01321-w

Bastian, M., Heymann, S., & Jacomy, M. (2009). Gephi: An Open Source Software for Exploring and Manipulating Networks. *Proceedings of the International AAAI Conference on Web and Social Media*, *3*(1), 361–362. https://doi.org/10.1609/icwsm.v3i1.13937

Basu, N. B., Thompson, S. E., & Rao, P. S. C. (2011). Hydrologic and biogeochemical functioning of intensively managed catchments: A synthesis of top-down analyses: Managed catchments. *Water Resources Research*, *47*(10).

https://doi.org/10.1029/2011WR010800

Berhe, A. A., & Torn, M. S. (2017). Erosional redistribution of topsoil controls soil nitrogen dynamics. *Biogeochemistry*, *132*(1–2), 37–54. https://doi.org/10.1007/s10533-016-0286-5

Bormann, F. H., & Likens, G. E. (1967). Small watersheds can provide invaluable information about terrestrial ecosystems., *155*, 7.

Bourgeois, I., Clément, J., Caillon, N., & Savarino, J. (2019). Foliar uptake of atmospheric nitrate by two dominant subalpine plants: insights from *in situ* triple-isotope analysis. *New Phytologist*, *223*(4), 1784–1794. https://doi.org/10.1111/nph.15761

Bouskill, N. J., Conrad, M. E., Bill, M., Brodie, E. L., Cheng, Y., Hobson, C., et al. (2019). Evidence for Microbial Mediated NO3− Cycling Within Floodplain Sediments During Groundwater Fluctuations. *Frontiers in Earth Science*, *7*, 189. https://doi.org/10.3389/feart.2019.00189

Brookshire, E. N. J., Valett, H. M., & Gerber, S. (2009). Maintenance of terrestrial nutrient loss signatures during in-stream transport. *Ecology*, *90*(2), 293–299. https://doi.org/10.1890/08-0949.1

Campbell, D. H., Kendall, C., Chang, C. C. Y., Silva, S. R., & Tonnessen, K. A. (2002). Pathways for nitrate release from an alpine watershed: Determination using $\delta^{15}N$ and $\delta^{18}O$: ALPINE WATERSHED NITRATE $\delta^{15}N$ AND $\delta^{18}O$. *Water Resources Research*, *38*(5), 10-1-10–9. https://doi.org/10.1029/2001WR000294

Carnevali, P. B. M., Lavy, A., Thomas, A. D., Crits-Christoph, A., Diamond, S., Meéheust, R., et al. (2020). *Meanders as a scaling motif for understanding of floodplain soil microbiome* *and biogeochemical potential at the watershed scale* (preprint). Microbiology. https://doi.org/10.1101/2020.05.14.086363

Carroll, R. W. H., Gochis, D., & Williams, K. H. (2020). Efficiency of the Summer Monsoon in Generating Streamflow Within a Snow-Dominated Headwater Basin of the Colorado River. *Geophysical Research Letters*, *47*(23). https://doi.org/10.1029/2020GL090856

Carroll, Rosemary, Newman, Alexander, Beutler, Curtis, and Williams, Kenneth. (2021). Stream discharge data collected within the East River, Colorado for the Lawrence Berkeley National Laboratory Watershed Function Science Focus Area (water years 2019 to 2020). doi:10.15485/1779721.

Casciotti, K. L., Sigman, D. M., Hastings, M. G., Böhlke, J. K., & Hilkert, A. (2002). Measurement of the Oxygen Isotopic Composition of Nitrate in Seawater and Freshwater Using the Denitrifier Method. *Analytical Chemistry*, *74*(19), 4905–4912. https://doi.org/10.1021/ac020113w

Clark, S. C., Barnes, R. T., Oleksy, I. A., Baron, J. S., & Hastings, M. G. (2021). Persistent Nitrate in Alpine Waters with Changing Atmospheric Deposition and Warming Trends. *Environmental Science & Technology*, *55*(21), 14946–14956. https://doi.org/10.1021/acs.est.1c02515

Condon, L. E., Atchley, A. L., & Maxwell, R. M. (2020). Evapotranspiration depletes groundwater under warming over the contiguous United States. *Nature Communications*, *11*(1), 873. https://doi.org/10.1038/s41467-020-14688-0

Craine, J. M., Elmore, A. J., Wang, L., Aranibar, J., Bauters, M., Boeckx, P., et al. (2018). Isotopic evidence for oligotrophication of terrestrial ecosystems. *Nature Ecology & Evolution*, *2*(11), 1735–1744. https://doi.org/10.1038/s41559-018-0694-0

Fahey, T. J., Yavitt, J. B., Pearson, J. A., & Knight, D. H. (1985). The nitrogen cycle in lodgepole pine forests, southeastern Wyoming. *Biogeochemistry*, *1*(3), 257–275. https://doi.org/10.1007/BF02187202

Finlay, R. D., Frostegard, A., & Sonnerfeldt, A.-M. (1992). Utilization of organic and inorganic nitrogen sources by ectomycorrhizal fungi in pure culture and in symbiosis with Pinus contorta Dougl. ex Loud. *New Phytologist*, *120*(1), 105–115. https://doi.org/10.1111/j.1469-8137.1992.tb01063.x

Fox, P. M., Carrero, S., Anderson, C., Dewey, C., Keiluweit, M., Conrad, M., et al. (2022). Sulfur Biogeochemical Cycling and Redox Dynamics in a Shale-Dominated Mountainous Watershed. *Journal of Geophysical Research: Biogeosciences*, *127*(6). https://doi.org/10.1029/2021JG006769

Godsey, S. E., Kirchner, J. W., & Clow, D. W. (2009). Concentration-discharge relationships reflect chemostatic characteristics of US catchments. *Hydrological Processes*, *23*(13), 1844–1864. https://doi.org/10.1002/hyp.7315

Gomez-Velez, J. D., Harvey, J. W., Cardenas, M. B., & Kiel, B. (2015). Denitrification in the Mississippi River network controlled by flow through river bedforms. *Nature Geoscience*, *8*(12), 941–945. https://doi.org/10.1038/ngeo2567

Goodale, C. L. (2017). Multiyear fate of a ^{15}N tracer in a mixed deciduous forest: retention, redistribution, and differences by mycorrhizal association. *Global Change Biology*, *23*(2), 867–880. https://doi.org/10.1111/gcb.13483

Gosz, J. R. (1981). Nitrogen cycling in coniferous forests. *Ecological Bulletins*, *30*, 405–426.

Granger, J., & Wankel, S. D. (2016). Isotopic overprinting of nitrification on denitrification as a ubiquitous and unifying feature of environmental nitrogen cycling. *Proceedings of the*

National Academy of Sciences, *113*(42), E6391–E6400. https://doi.org/10.1073/pnas.1601383113

Gurmesa, G. A., Wang, A., Li, S., Peng, S., de Vries, W., Gundersen, P., et al. (2022). Retention of deposited ammonium and nitrate and its impact on the global forest carbon sink. *Nature Communications*, *13*(1), 880. https://doi.org/10.1038/s41467-022-28345-1

Hobbie, E. A., & Högberg, P. (2012). Nitrogen isotopes link mycorrhizal fungi and plants to nitrogen dynamics. *New Phytologist*, *196*(2), 367–382. https://doi.org/10.1111/j.1469-8137.2012.04300.x

Holloway, J M, Dahlgren, R. A., Hansen, B., & Casey, W. H. (1998). Contribution of bedrock nitrogen to high nitrate concentrations in stream water. *Nature*, *395*, 4.

Holloway, JoAnn M., & Dahlgren, R. A. (2002). Nitrogen in rock: Occurrences and biogeochemical implications: BIOGEOCHEMICAL IMPLICATIONS OF N IN ROCK. *Global Biogeochemical Cycles*, *16*(4), 65-1-65–17. https://doi.org/10.1029/2002GB001862

Houlton, B. Z., Morford, S. L., & Dahlgren, R. A. (2018). Convergent evidence for widespread rock nitrogen sources in Earth's surface environment. *Science*, *360*(6384), 58–62. https://doi.org/10.1126/science.aan4399

Hubbard, S. S., Williams, K. H., Agarwal, D., Banfield, J., Beller, H., Bouskill, N., et al. (2018). The East River, Colorado, Watershed: A Mountainous Community Testbed for Improving Predictive Understanding of Multiscale Hydrological–Biogeochemical Dynamics. *Vadose Zone Journal*, *17*(1), 1–25. https://doi.org/10.2136/vzj2018.03.0061

Jia, M., Winkler, M. K. H., & Volcke, E. I. P. (2020). Elucidating the Competition between Heterotrophic Denitrification and DNRA Using the Resource-Ratio Theory.

Environmental Science and Technology, *54*(21), 13953–62. https://doi.org/10.1021/acs.est.0c01776

Johnson, H. M., & Stets, E. G. (2020). Nitrate in Streams During Winter Low-Flow Conditions as an Indicator of Legacy Nitrate. *Water Resources Research*, *56*(11). https://doi.org/10.1029/2019WR026996

Killham, K. (1990). Nitrification in coniferous forest soils. *Plant and Soil*, *128*(1), 31–44. https://doi.org/10.1007/BF00009394

Knapp, J. L. A., von Freyberg, J., Studer, B., Kiewiet, L., & Kirchner, J. W. (2020). Concentration–discharge relationships vary among hydrological events, reflecting differences in event characteristics. *Hydrology and Earth System Sciences*, *24*(5), 2561–2576. https://doi.org/10.5194/hess-24-2561-2020

Knapp, J. L. A., Li, L., & Musolff, A. (2022). Hydrologic connectivity and source heterogeneity control concentration–discharge relationships. *Hydrological Processes*, *36*(9). https://doi.org/10.1002/hyp.14683

Kou, D., Yang, G., Li, F., Feng, X., Zhang, D., Mao, C., et al. (2020). Progressive nitrogen limitation across the Tibetan alpine permafrost region. *Nature Communications*, *11*(1), 3331. https://doi.org/10.1038/s41467-020-17169-6

Kronzucker, H. J., Siddiqi, M. Y., & Glass, A. D. M. (1997). Conifer root discrimination against soil nitrate and the ecology of forest succession. *Nature*, *385*(6611), 59–61. https://doi.org/10.1038/385059a0

Lajtha, K. (2020). Nutrient retention and loss during ecosystem succession: revisiting a classic model. *Ecology*, *101*(1). https://doi.org/10.1002/ecy.2896

Lansdown, K., Heppell, C. M., Trimmer, M., Binley, A., Heathwaite, A. L., Byrne, P., & Zhang,

H. (2015). The interplay between transport and reaction rates as controls on nitrate attenuation in permeable, streambed sediments: Nitrate removal in permeable sediments. *Journal of Geophysical Research: Biogeosciences*, *120*(6), 1093–1109. https://doi.org/10.1002/2014JG002874

Leinweber, P., Kruse, J., Baum, C., Arcand, M., Knight, J. D., Farrell, R., et al. (2013). Advances in Understanding Organic Nitrogen Chemistry in Soils Using State-of-the-art Analytical Techniques. In *Advances in Agronomy* (Vol. 119, pp. 83–151). Elsevier. https://doi.org/10.1016/B978-0-12-407247-3.00002-0

Leonard, L. T., Mikkelson, K., Hao, Z., Brodie, E. L., Williams, K. H., & Sharp, J. O. (2020). A comparison of lodgepole and spruce needle chemistry impacts on terrestrial biogeochemical processes during isolated decomposition. *PeerJ*, *8*, e9538. https://doi.org/10.7717/peerj.9538

Li, D., Wrzesien, M. L., Durand, M., Adam, J., & Lettenmaier, D. P. (2017). How much runoff originates as snow in the western United States, and how will that change in the future? *Geophysical Research Letters*, *44*(12), 6163–6172. https://doi.org/10.1002/2017GL073551

Li, L., Sullivan, P. L., Benettin, P., Cirpka, O. A., Bishop, K., Brantley, S. L., et al. (2021). Toward catchment hydro-biogeochemical theories. *WIREs Water*, *8*(1). https://doi.org/10.1002/wat2.1495

Li, Y., Schichtel, B. A., Walker, J. T., Schwede, D. B., Chen, X., Lehmann, C. M. B., et al. (2016). Increasing importance of deposition of reduced nitrogen in the United States. *Proceedings of the National Academy of Sciences*, *113*(21), 5874–5879. https://doi.org/10.1073/pnas.1525736113

Maavara, T., Siirila-Woodburn, E. R., Maina, F., Maxwell, R. M., Sample, J. E., Chadwick, K. D., et al. (2021). Modeling geogenic and atmospheric nitrogen through the East River Watershed, Colorado Rocky Mountains. *PLOS ONE*, *16*(3), e0247907. https://doi.org/10.1371/journal.pone.0247907

Manning, A. H., Verplanck, P. L., Mast, M. L., & Wanty, R. B. (2008). Hydrogeochemical investigation of the Standard Mine vicinity, upper Elk Creek Basin, Colorado (Scientific Investigations Report). USGS.

Mason, R. E., Craine, J. M., Lany, N. K., Jonard, M., Ollinger, S. V., Groffman, P. M., et al. (2022). Evidence, causes, and consequences of declining nitrogen availability in terrestrial ecosystems. *Science*, *376*(6590), eabh3767. https://doi.org/10.1126/science.abh3767

McDonnell, J. J., Sivapalan, M., Vaché, K., Dunn, S., Grant, G., Haggerty, R., et al. (2007). Moving beyond heterogeneity and process complexity: A new vision for watershed hydrology: Opinion. *Water Resources Research*, *43*(7). https://doi.org/10.1029/2006WR005467

Michalski, G., Bhattacharya, S. K., & Mase, D. F. (2012). Oxygen Isotope Dynamics of Atmospheric Nitrate and Its Precursor Molecules. In M. Baskaran (Ed.), *Handbook of Environmental Isotope Geochemistry* (pp. 613–635). Berlin, Heidelberg: Springer Berlin Heidelberg. https://doi.org/10.1007/978-3-642-10637-8_30

Morford, S. L., Houlton, B. Z., & Dahlgren, R. A. (2011). Increased forest ecosystem carbon and nitrogen storage from nitrogen rich bedrock. *Nature*, *477*(7362), 78–81. https://doi.org/10.1038/nature10415

Moyes, A. B., Kueppers, L. M., Pett-Ridge, J., Carper, D. L., Vandehey, N., O'Neil, J., & Frank,

A. C. (2016). Evidence for foliar endophytic nitrogen fixation in a widely distributed subalpine conifer. *New Phytologist*, *210*(2), 657–668. https://doi.org/10.1111/nph.13850

Musolff, A., Schmidt, C., Selle, B., & Fleckenstein, J. H. (2015). Catchment controls on solute export. *Advances in Water Resources*, *86*, 133–146. https://doi.org/10.1016/j.advwatres.2015.09.026

Nardi, P., Laanbroek, H. J., Nicol, G. W., Renella, G., Cardinale, M., Pietramellara, G., et al. (2020). Biological nitrification inhibition in the rhizosphere: determining interactions and impact on microbially mediated processes and potential applications. *FEMS Microbiology Reviews*, *44*(6), 874–908. https://doi.org/10.1093/femsre/fuaa037

Newcomer, M. E., Bouskill, N. J., Wainwright, H., Maavara, T., Siirila-Woodburn, E. R., Dwivedi, D., et al. (2021). Hysteresis Patterns of Watershed Nitrogen Retention and Loss Over the Past 50 years in United States Hydrological Basins. *Global Biogeochemical Cycles*, 28.

Pelletier, J. D., Barron-Gafford, G. A., Gutiérrez-Jurado, H., Hinckley, E.-L. S., Istanbulluoglu, E., McGuire, L. A., et al. (2018). Which way do you lean? Using slope aspect variations to understand Critical Zone processes and feedbacks: Which way do you lean? *Earth Surface Processes and Landforms*, *43*(5), 1133–1154. https://doi.org/10.1002/esp.4306

Peterson, B. J. (2001). Control of Nitrogen Export from Watersheds by Headwater Streams. *Science*, *292*(5514), 86–90. https://doi.org/10.1126/science.1056874

Phillips, R. P., Brzostek, E., & Midgley, M. G. (2013). The mycorrhizal-associated nutrient economy: a new framework for predicting carbon–nutrient couplings in temperate forests. *New Phytologist*, *199*(1), 41–51. https://doi.org/10.1111/nph.12221

Pinay, G., Peiffer, S., De Dreuzy, J.-R., Krause, S., Hannah, D. M., Fleckenstein, J. H., et al.

(2015). Upscaling Nitrogen Removal Capacity from Local Hotspots to Low Stream Orders' Drainage Basins. *Ecosystems*, *18*(6), 1101–1120. https://doi.org/10.1007/s10021-015-9878-5

Rogers, D. B., Newcomer, M. E., Raberg, J. H., Dwivedi, D., Steefel, C., Bouskill, N., et al. (2021). Modeling the Impact of Riparian Hollows on River Corridor Nitrogen Exports. *Frontiers in Water*, *3*, 590314. https://doi.org/10.3389/frwa.2021.590314

Rose, L. A., Elliott, E. M., & Adams, M. B. (2015). Triple Nitrate Isotopes Indicate Differing Nitrate Source Contributions to Streams Across a Nitrogen Saturation Gradient. *Ecosystems*, *18*(7), 1209–1223. https://doi.org/10.1007/s10021-015-9891-8

Ruddell, B. L., & Kumar, P. (2009). Ecohydrologic process networks: 2. Analysis and characterization: Ecohydrologic process networks, 2. *Water Resources Research*, *45*(3). https://doi.org/10.1029/2008WR007280

Schimel, D. S., Braswell, B. H., & Parton, W. J. (1997). Equilibration of the terrestrial water, nitrogen, and carbon cycles. *Proceedings of the National Academy of Sciences*, *94*(16), 8280–8283. https://doi.org/10.1073/pnas.94.16.8280

Sebestyen, S. D., Shanley, J. B., Boyer, E. W., Kendall, C., & Doctor, D. H. (2014). Coupled hydrological and biogeochemical processes controlling variability of nitrogen species in streamflow during autumn in an upland forest: Stream N dynamics during autumn. *Water Resources Research*, *50*(2), 1569–1591. https://doi.org/10.1002/2013WR013670

Sebestyen, S. D., Ross, D. S., Shanley, J. B., Elliott, E. M., Kendall, C., Campbell, J. L., et al. (2019). Unprocessed Atmospheric Nitrate in Waters of the Northern Forest Region in the U.S. and Canada. *Environmental Science & Technology*, *53*(7), 3620–3633. https://doi.org/10.1021/acs.est.9b01276

Sigman, D. M., Casciotti, K. L., Andreani, M., Barford, C., Galanter, M., & Böhlke, J. K. (2001). A Bacterial Method for the Nitrogen Isotopic Analysis of Nitrate in Seawater and Freshwater. *Analytical Chemistry*, *73*(17), 4145–4153. https://doi.org/10.1021/ac010088e

Siirila-Woodburn, E. R., Rhoades, A. M., Hatchett, B. J., Huning, L. S., Szinai, J., Tague, C., et al. (2021). A low-to-no snow future and its impacts on water resources in the western United States. *Nature Reviews Earth & Environment*, *2*(11), 800–819. https://doi.org/10.1038/s43017-021-00219-y

Sorensen, P. O., Beller, H. R., Bill, M., Bouskill, N. J., Hubbard, S. S., Karaoz, U., et al. (2020). The Snowmelt Niche Differentiates Three Microbial Life Strategies That Influence Soil Nitrogen Availability During and After Winter. *Frontiers in Microbiology*, *11*, 871. https://doi.org/10.3389/fmicb.2020.00871

Sprenger, M., Carroll, R. W. H., Dennedy-Frank, J., Siirila-Woodburn, E. R., Newcomer, M. E., Brown, W., et al. (2022). Variability of Snow and Rainfall Partitioning Into Evapotranspiration and Summer Runoff Across Nine Mountainous Catchments. *Geophysical Research Letters*, *49*(13). https://doi.org/10.1029/2022GL099324

Steffen, W., Richardson, K., Rockström, J., Cornell, S. E., Fetzer, I., Bennett, E. M., et al. (2015). Planetary boundaries: Guiding human development on a changing planet. *Science*, *347*(6223), 1259855. https://doi.org/10.1126/science.1259855

Tokunaga, T. K., Tran, A. P., Wan, J., Dong, W., Newman, A. W., Beutler, C. A., Brown, W., Henderson, A. N., Williams, K. H. (2022). Quantifying subsurface flow and solute transport in a snowmelt-recharged hillslope with multiyear water balance. Water Resources Research, 58, *e2022WR032902. https://doi.org/10.1029/2022WR032902*

Thébault, A., Clément, J.-C., Ibanez, S., Roy, J., Geremia, R. A., Pérez, C. A., et al. (2014).

Nitrogen limitation and microbial diversity at the treeline. *Oikos*, *123*(6), 729–740. https://doi.org/10.1111/j.1600-0706.2013.00860.x

Thompson, S. E., Basu, N. B., Lascurain, J., Aubeneau, A., & Rao, P. S. C. (2011). Relative dominance of hydrologic versus biogeochemical factors on solute export across impact gradients: Hydrology controls solute export. *Water Resources Research*, *47*(10). https://doi.org/10.1029/2010WR009605

Uhlemann, S., Dafflon, B., Wainwright, H. M., Williams, K. H., Minsley, B., Zamudio, K., et al. (2022). Surface parameters and bedrock properties covary across a mountainous watershed: Insights from machine learning and geophysics. *Science Advances*, *8*(12), eabj2479. https://doi.org/10.1126/sciadv.abj2479

Wainwright, H. M., Uhlemann, S., Franklin, M., Falco, N., Bouskill, N. J., Newcomer, M. E., et al. (2022). Watershed zonation through hillslope clustering for tractably quantifying above- and below-ground watershed heterogeneity and functions. *Hydrology and Earth System Sciences*, *26*(2), 429–444. https://doi.org/10.5194/hess-26-429-2022

Walker, J. T., Beachley, G., Amos, H. M., Baron, J. S., Bash, J., Baumgardner, R., et al. (2019). Toward the improvement of total nitrogen deposition budgets in the United States. *Science of The Total Environment*, *691*, 1328–1352. https://doi.org/10.1016/j.scitotenv.2019.07.058

Wan, J., Tokunaga, T. K., Williams, K. H., Dong, W., Brown, W., Henderson, A. N., et al. (2019). Predicting sedimentary bedrock subsurface weathering fronts and weathering rates. *Scientific Reports*, *9*(1), 17198. https://doi.org/10.1038/s41598-019-53205-2

Wan, J., Tokunaga, T. K., Brown, W., Newman, A. W., Dong, W., Bill, M., et al. (2020). Bedrock weathering contributes to subsurface reactive nitrogen and nitrous oxide emissions. *Nature Geoscience*, (14), 217–224. https://doi.org/10.1038/s41561-021-00717-0

Ward, E. B., Duguid, M. C., Kuebbing, S. E., Lendemer, J. C., & Bradford, M. A. (2022). The functional role of ericoid mycorrhizal plants and fungi on carbon and nitrogen dynamics in forests. *New Phytologist*, 18.

Webb, R. W., Wigmore, O., Jennings, K., Fend, M., & Molotch, N. P. (2020). Hydrologic connectivity at the hillslope scale through intra-snowpack flow paths during snowmelt. *Hydrological Processes*, *34*(7), 1616–1629. https://doi.org/10.1002/hyp.13686

Wexler, S. K., Goodale, C. L., McGuire, K. J., Bailey, S. W., & Groffman, P. M. (2014). Isotopic signals of summer denitrification in a northern hardwood forested catchment. *Proceedings of the National Academy of Sciences*, *111*(46), 16413–16418. https://doi.org/10.1073/pnas.1404321111

Winnick, M. J., Carroll, R. W. H., Williams, K. H., Maxwell, R. M., Dong, W., & Maher, K. (2017). Snowmelt controls on concentration-discharge relationships and the balance of oxidative and acid-base weathering fluxes in an alpine catchment, East River, Colorado: Acid-base versus oxidative weathering fluxes. *Water Resources Research*, *53*(3), 2507–2523. https://doi.org/10.1002/2016WR019724

Woelber, B., Maneta, M. P., Harper, J., Jencso, K. G., Gardner, W. P., Wilcox, A. C., & López-Moreno, I. (2018). The influence of diurnal snowmelt and transpiration on hillslope throughflow and stream response. *Hydrology and Earth System Sciences*, *22*(8), 4295–4310. https://doi.org/10.5194/hess-22-4295-2018

Yuan, K., Zhu, Q., Li, F., Riley, W. J., Torn, M., Chu, H., et al. (2022). Causality guided machine learning model on wetland CH4 emissions across global wetlands. *Agricultural* *and Forest Meteorology*, *324*, 109115. https://doi.org/10.1016/j.agrformet.2022.109115

Zhi, W., & Li, L. (2020). The Shallow and Deep Hypothesis: Subsurface Vertical Chemical Contrasts Shape Nitrate Export Patterns from Different Land Uses. *Environmental Science & Technology*, acs.est.0c01340. https://doi.org/10.1021/acs.est.0c01340

Zhi, W., Li, L., Dong, W., Brown, W., Kaye, J., Steefel, C., & Williams, K. H. (2019). Distinct Source Water Chemistry Shapes Contrasting Concentration-Discharge Patterns. *Water Resources Research*, 2018WR024257. https://doi.org/10.1029/2018WR024257

Zhi, W., Williams, K. H., Carroll, R. W. H., Brown, W., Dong, W., Kerins, D., & Li, L. (2020). Significant stream chemistry response to temperature variations in a high-elevation mountain watershed. *Communications Earth & Environment*, *1*(1), 43. https://doi.org/10.1038/s43247-020-00039-w

Zhou, X., Wang, A., Hobbie, E. A., Zhu, F., Qu, Y., Dai, L., et al. (2021). Mature conifers assimilate nitrate as efficiently as ammonium from soils in four forest plantations. *New Phytologist*, *229*(6), 3184–3194. https://doi.org/10.1111/nph.17110

Zhu, Q., Castellano, M. J., & Yang, G. (2018). Coupling soil water processes and the nitrogen cycle across spatial scales: Potentials, bottlenecks and solutions. *Earth-Science Reviews*, *187*, 248–258. https://doi.org/10.1016/j.earscirev.2018.10.005

Zogg, G. P., Zak, D. R., Pregitzer, K. S., & Burton, A. J. (2000). Microbial immobilization and the retention of anthropogenic nitrate in a Northern hardwood forest. *Ecology*, *81*(7), 1858–1866. https://doi.org/10.1890/0012-9658(2000)081[1858:MIATRO]2.0.CO;2